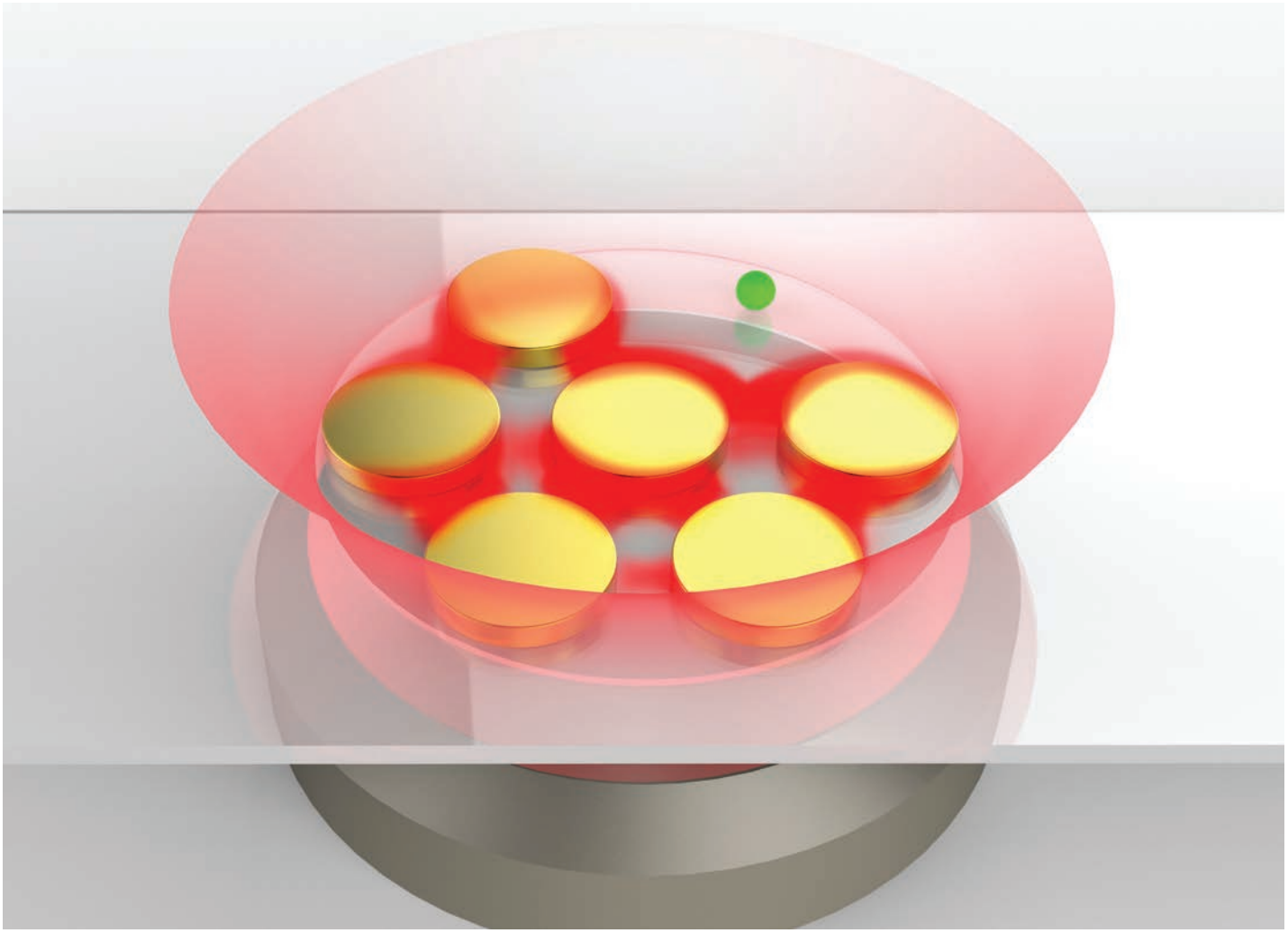

Showcasing research from the College of Electronic Engineering, South China Agricultural University, Guangzhou, China.

Title: Single protein sensing with asymmetric plasmonic hexamer *via* Fano resonance enhanced two-photon luminescence

An experimental scheme to realize the single-protein sensing by using two-photon luminescence enhanced by a plasmonic Fano resonance system is proposed. The moving directions and the spatial locations of a protein can be detected *via* its far field two-photon luminescence, which benefits from the resonant near-field interaction with the electromagnetic hot-spots supported by the asymmetric plasmonic hexamer. The sensitivity to changes in position of our method is substantially better than the conventional linear sensing approach utilizing Fano resonance.

As featured in:

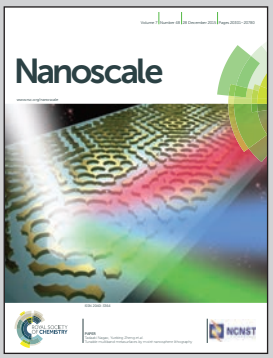

See Yi Xu, Andrey E. Miroshnichenko *et al.* *Nanoscale*, 2015, **7**, 20405.

ROYAL SOCIETY OF CHEMISTRY

www.rsc.org/nanoscale

Registered charity number: 207890

Nanoscale

PAPER

View Article Online
View Journal | View Issue

Cite this: *Nanoscale*, 2015, **7**, 20405

Single protein sensing with asymmetric plasmonic hexamer *via* Fano resonance enhanced two-photon luminescence†

Hai-Dong Deng,[a] Xing-Yu Chen,[a] Yi Xu*[b] and Andrey E. Miroshnichenko*[c]

Received 21st June 2015,
Accepted 18th September 2015

DOI: 10.1039/c5nr04118j

www.rsc.org/nanoscale

Fano resonances in plasmonic systems have been proved to facilitate various sensing applications in the nanoscale. In this work, we propose an experimental scheme to realize a single protein sensing by utilizing its two-photon luminescence enhanced by a plasmonic Fano resonance system. The asymmetric gold hexamer supporting polarization-dependent Fano resonances and plasmonic modes without in-plane rotational symmetry is used as a referenced spatial coordinate for bio-sensing. We demonstrate *via* the full-vectorial three-dimensional simulation that the moving direction and the spatial location of a protein can be detected *via* its two-photon luminescence, which benefits from the resonant near-field interaction with the electromagnetic hot-spots. The sensitivity to changes in position of our method is substantially better compared with the conventional linear sensing approach. Our strategy would facilitate the sensing, tracking and imaging of a single biomolecule in deep sub-wavelength scale and with a small optical extinction cross-section.

1 Introduction

Single-molecule detection received tremendous attention in recent years due to its importance in molecular biology and materials science.[1–5] There are several methods to achieve the single-molecule bio-sensing, such as laser-induced fluorescence,[6] surface-enhanced Raman scattering,[7] photothermal method,[8] standard modulation-free absorption measurements,[9] stimulated emission,[10] resonant optical cavity[11,12] and the recently demonstrated method based on the photonic nanojet produced by the micro dielectric sphere array.[13] Providing the possibility to detect and visualize molecules at the same time, fluorescence spectroscopy based bio-sensing is one of the long standing methods for single-molecule detection.[6]

However, if the target is in deep subwavelength scale or with a tiny optical extinction cross-section, amplification of the detected signal is needed because the fluorescence signal from the nanoscale target is very weak. In that case, increasing the excitation rate of the analyte is one of the methods to amplify the fluorescence signal.[13] Localized surface plasmon resonance (LSPR) has been regarded as a solution to enhance the local electric field while it still maintains the size of bio-sensing probe in the subwavelength scale at the same time.[14–19] Therefore, the fluorescence enhancement can be tailored by the plasmonic mode supported by metallic nanoparticles.[20,21] Such fluorescence enhancement can be maximized when the wavelength of the excitation laser and the emission spectrum of the dye overlap with the LSPR.[22] It was demonstrated that photoluminescence of an individual gold nanorod can be used to detect biological molecule binding events.[23–25] Alternatively, the distance-dependent fluorescence of molecules bound to silica-coated gold nanorods can be used for bio-sensing.[26]

Of particular interest in bio-sensing is that the motion of a single protein can be detected and traced.[27] It could provide us with the useful information of the biokinetics at the single molecule level. To date, it is very difficult to trace the nano-analyte by the conventional fluorescence labelling because of the optical diffraction limit. Tracing the two-photon luminescence (TPL) signal from a gold nanorod can be used to detect the moving direction, position, size, and material type of nanoparticles,[28] providing an alternative for detecting nanoparticles *via* far-field luminescence signals. However, because the plasmonic mode of a gold nanorod possesses two-fold rotational symmetry when the excitation polarization is parallel to the long axis of the nanorod, the near-field coupling between the

[a]*College of Electronic Engineering, South China Agricultural University, Guangzhou, 510642, P.R. China*
[b]*Department of Electronic Engineering, College of Information Science and Technology, Jinan University, Guangzhou 510632, P.R. China. E-mail: e_chui@qq.com*
[c]*Nonlinear Physics Centre, Australian National University, Acton, ACT 2601, Australia. E-mail: andrey.miroshnichenko@anu.edu.au*
†Electronic supplementary information (ESI) available. See DOI: 10.1039/C5NR04118J

nanorod and the analyte is the same in the directions mirrored by the long axis of gold nanorod. Therefore, this method is limited and cannot be used to distinguish degenerated directions referring to the gold nanorod. In order to fully explore the moving directions referring to the center of the plasmonic sensor, one should break the rotational symmetry of the plasmonic mode involved in the bio-sensing.

By employing a plasmonic Fano resonance,[29–33] in which the destructive interference between a super-radiant mode and a subradiant mode relieves the radiative damping of the LSPR, the local field can be further enhanced. It is demonstrated recently that the figures of merit of the refractive index sensing based on plasmonic Fano resonance has almost beaten the theoretical limit.[34] At the same time, plasmonic Fano resonance is not only capable of enhancing the sensitivity of the conventional plasmonic sensing,[29–33] but also of enhancing the luminescence signals compared with simple plasmonic particles.[35–37] As a result, seeking a plasmonic Fano resonant system possessing electromagnetic modes without in-plane rotational symmetry is crucial to fully obtain the spatial binding kinetics of a subwavelength fluorescent protein.

In this paper, we propose a Fano resonance enhanced TPL strategy to sense the moving direction and the spatial location of a single protein using an asymmetric plasmonic hexamer (APH). Such a plasmonic system supports Fano resonance modes without rotational symmetry. When the protein locates at different spatial locations above the plasmonic system, it would interact with the collective oscillated free charges of the plasmonic system *via* Coulomb interactions, leading to a resonant-like enhancement of electric field inside the protein. Detecting the variation of the enhanced TPL signal from the protein provides us an opportunity to sense the spatial locations of the protein. Our full-vectorial electromagnetic simulations validate the high sensitivity of our method compared with the conventional one utilizing Fano resonance.

2 Results

The plasmonic oligomer system has been proved to be a superior nanoscale platform for manipulating Fano resonance.[38–61] Nowadays, it becomes a popular tool widely applied in biology, chemistry and physics.[29–33] For a plasmonic oligomer with rotational symmetry, the supported Fano resonances are polarization-independent.[43,62] If the symmetry of the structure is broken, the Fano resonance of the system becomes polarization-dependent.[43] More importantly, the collective oscillation of the free charges driven by the incident polarization will be affected by the asymmetry structure, leading to the formation of asymmetric plasmonic modes without any in-plane rotational symmetry. Such asymmetric modes can be used to engineer the near-field hot-spots distribution with the excitation polarization. Meanwhile, the asymmetric near field distribution can be regarded as a reference spatial grid to identify the spatial locations of the protein. It was also demonstrated that plasmonic oligomer systems can be used to enhance nonlinear processes even without employing Fano resonance,[63] which implies a chance to obtain further enhancement by utilizing plasmonic Fano resonance for the nonlinear bio-sensing.[64] In the following, we choose the APH as an example to demonstrate the single protein sensing using the TPL of the protein enhanced by the Fano resonance.

The proposed experimental scheme is shown in Fig. 1(a). The APH is formed by removing a satellitic nanodisk from a six-folded heptamer. The green sphere indicates the protein under detection. The plasmonic structure is excited with a femtosecond laser pulse focused by the 100× objective lens of an inverted fluorescence microscope and the TPL signal of the protein is collected by the same objective lens. Bandpass filter can be applied after the objective lens to specify the wavelength range of the collected TPL. There is a suitable power range of the femtosecond pulse to generate effective TPL without melting the metallic structure[65–67] and avoid the photobleaching effect.[68] As a result, we do not consider the metal fusion effect and the photobleaching effect in the simulation. In the numerical modelling, we use a refractive index $n = 1.5$ and a diameter $d = 10$ nm to numerically model a green florescence protein (GFP). More details for the numerical modelling can be found in the Methods section. Fig. 1(b) and (c) present the calculated absorption and the scattering-cross sections of the APH shown in Fig. 1(a) under different excitation polarizations indicated in corresponding insets. It should be emphasized that the vertical polarization is corresponding to $P = 0°$. We only plot several representative cases and neglect results of degenerated polarization directions. These results demonstrate that Fano resonances of the APH are polarization-dependent. In Fig. 1(d) and (e), we show the corresponding electric intensity distribution $|E|^2$ at two absorption peaks for $\lambda = 920$ nm ($P = 0°$) and $\lambda = 820$ nm ($P = 120°$). The excitation polarizations are indicated by red double arrows in their insets. One can clearly see that the near-field hot-spots distribution in Fig. 1(d) is more asymmetric than the one in Fig. 1(e), which still possesses a mirror symmetry. We present the charge orientations of the subradiant states in the ESI Fig. S1(a)† which are important for the observation of Fano resonance. As can be seen from the charged distributions of these subradiant modes (~820 nm and ~920 nm), they are distinct from each other by their constituent dipole orientations of the APH. For the case in Fig. 1(e), the dipole moments in the gold disks along the symmetry axis of the APH are parallel with the collective dipoles driven by the excitation polarization ($P = 120°$). Therefore, the near field hot-spot distributions in Fig. 1(e) still possesses mirror symmetry. While the interference between the collective dipoles driven by the excitation polarization ($P = 0°$) and the subradiant state near 920 nm leads to a hot spots distribution without rotational symmetry. We also present the electric intensity distributions of the representative excitation polarizations in the ESI Fig. S1(b).† The hot spot distribution can be classified into two categories referring to the dominant subradiant states. Different excitation polarizations of the plane waves would have different orientations of the collective dipoles and thus distinct interference results with these

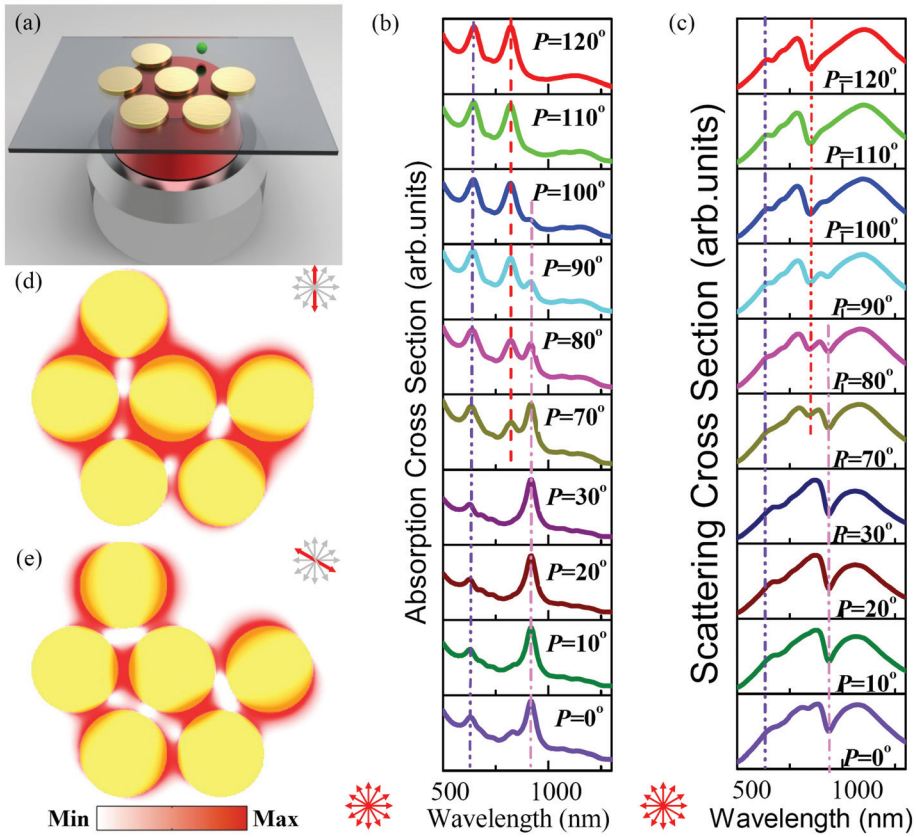

Fig. 1 (a) The proposed sketch of the experimental setup for the single protein sensing with an asymmetric plasmonic hexamer. The thickness and the radius of the nanodisk are 30 nm and 64 nm, respectively. The gaps between neighbouring nanodisks are 15 nm and the single protein (n = 1.5) is 10 nm in diameter. It should be noted that the size of objective lens and focused laser beam are reduced referring to the APH for better visualization. (b) Absorption and (c) scattering cross-sections of APH under the different excitation conditions. The corresponding polarizations are indicated by red double arrows in the insets. The APH is immersed in water (n = 1.33). (d) and (e) Are the bird's eye view of the three-dimensional electric intensity distribution $|E|^2$ at the most prominent peaks [λ = 920 nm for (d) and λ = 820 nm for (e)] of the absorption cross section under different excitations of polarizations. The color scales are saturated at the same degree for (d) and (e).

subradiant modes. Therefore, the strengths of the hot spot in one category can also be different owing to the distinct orientation of the superradiant states, as validated in the ESI Fig. S1.†

A GFP with a typical size smaller than 10 nm does not support any resonant mode in the considered spectrum and it can be regarded as a very small dielectric perturbation to the plasmonic system. Therefore, the magnitude of the electric field inside the protein is very small when it is excited directly by the laser, hampering the direct detection by the conventional fluorescence method. However, when the protein locates at a hotspot of the plasmonic mode, the polarization charges of the protein would interact with the free charge of the APH through Coulomb interactions. Therefore, the polarization charge would oscillate at the frequency similar to the LSPR, leading to a Fano resonant enhancement of the electric field inside the protein. As a result, TPL from the protein can thus be greatly enhanced compared with the case without the plasmonic structure. Because the hot-spots are distributed above the APH [see Fig. 1(d)], it means that a protein would encounter different scenarios of electric field fluctuation when it moves along different directions towards the APH's center. Such asymmetry mode provides a spatial grid to locate the subwavelength target, which is difficult to realize by the conventional diffraction-limited fluorescence method. Such difference is magnified by the $|E|^4$ dependence of TPL. Therefore, the spatial movement of the protein can be detected.

In the following, we choose one of the cases which supports the asymmetric hot-spot distribution [Fig. 1(d)] to demonstrate the single protein sensing *via* Fano resonance enhanced TPL. We consider a protein moving along a direction with an angle θ with respect to the symmetry axis of the structure (marked by a dashed line in Fig. 2(a)) just above the APH. It was demonstrated that the TPL spectra of coupled plasmonic systems can be manipulated by the structure parameters.[65–67] While the dominant TPL spectrum of the protein can be controlled by the genetic technology, such as the cyan florescence protein, yellow florescence protein and red florescence protein. It means that the peak wavelengths of TPL signals from typical proteins and the gold APH can be intentionally separated,

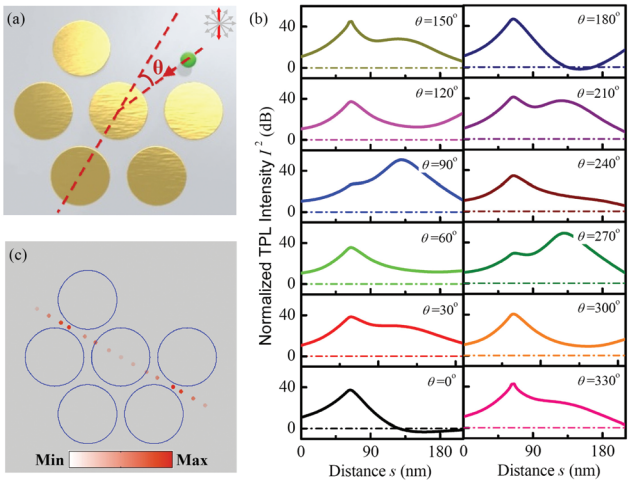

Fig. 2 (a) Sketch map of the sensing process. The input polarization is indicated by the red double arrows of the inset. (b) Evolutions of the normalized TPL intensity of the protein (solid line) when the protein moves along the surface of the APH at different directions (referring to different θ). It is normalized by the TPL of the protein without the APH under the same excitation condition. The corresponding evolutions of the normalized TPL intensity of the gold APH are shown by dotted dash-lines. It is normalized by the TPL of the APH without the protein under the same excitation condition. The normalized TPL is evaluated by using the eqn (2) in the Method section. (c) The evolutions of the square of electric intensity $|E|^4$ when the protein move along the surface of the APH at θ = 90°. It is excited at the resonant absorption wavelength λ = 820 nm. (b) and (c) Are both in logarithmic scale.

which would prevent the TPL of protein from being overwhelming by the one from gold APH. Therefore, we can detect their TPL signals in different spectrum windows. As the TPL is proportional to the volume integration of $|E|^4$ at the excitation frequency and the volume integration of $|E|^2$ at the emission frequency,[28] we can evaluate the corresponding TPL signals of the single protein and the gold APH numerically. Details of the modelling method can be found in the Methods section. We use the normalized TPL to account for the variation of the sensing signal. The TPL of the protein and the APH immersed in water under similar excitation conditions are used for the normalization, respectively. The APH's TPL is expected to have negligible fluctuation because of a very small refractive index of the protein n = 1.5. In other words, the protein does not add any new mode to the APH system which hampers it to be detected with the conventional sensing method even when the protein locates at hot-spots of the APH.[53] In contrast, the plasmonic Fano resonance enhanced local electric field would polarize the protein and render it to obtain giant enhancement of the electric field $|E|^4$ inside its volume. This is one of the key mechanisms involved in our scheme to detect the protein. Fig. 2(b) present the evolution of the normalized TPL from the protein when it moves to the center of the APH at different directions (θ). Definition of the normalized TPL can be found in the Method section. The fluctuation contrast of the TPL from the protein can be larger than five orders of magnitude. Such a big contrast would strengthen our strategy for detecting the kinetics of a single protein against fabrication impurity of the APH structure, which will be addressed below. Furthermore, distinct luminescence enhancement scenarios of the protein moving at different directions provide the base for distinguishing the motion of the protein, which benefits from the asymmetry nature of the plasmonic mode. Spatial locations of the protein can also be obtained by using the distance dependent TPL signals at given directions. This is the other mechanism involved in our sensing strategy. As can be seen from Fig. 1(d), the near-field hot-spots are more asymmetric compared to the dipole mode of a gold nanorod. Therefore, we can distinguish more directions than that in ref. 28. In addition, the sensitivity of our method benefits from the Fano resonance enhancement compared with their dipole resonance.[28,37] As a comparison, the maximum resonant wavelength shift of the conventional sensing strategy utilizing Fano resonance caused by the protein is less than 1 nm. As can be seen from the quantitative results shown in the ESI Fig. S2,† the variation of the linear sensing method based on Fano resonance is too small to be detected, implying that the conventional method would not be able to detect the position of the protein. Our sensitivity in position tracking is at least 50 dB better than the conventional sensing method (see Fig. 2 and ESI Fig. S2†). In order to obtain further understanding of the sensing process, we plot the square of the electric intensity $|E|^4$ of the protein above the APH when it moves at the direction θ = 90° in Fig. 2(c). Comparing the results of Fig. 2(c) with Fig. 1(d), we can conclude that two-photon absorption is enhanced in the vicinity of the hot-spots. Such a near-field interaction would induce giant enhancement of the electric field inside the protein at the excitation frequency of TPL though the protein itself does not support any resonant mode at this frequency. It should be noted that the APH also supports Fano resonance with a symmetric hot-spots distribution, as shown in Fig. 1(e). Fig. 3 presents the TPL sensing results for three pairs of degenerated moving directions (θ = 30° and θ = 330°, θ = 90° and θ = 270°, θ = 150° and θ = 210°), mirrored by the direction of θ = 0°. The TPL signals of each pair are the same when the protein is moving along such directions, which means that we cannot distinguish such degenerated moving directions. It can be concluded from these results that the exciting polarization of the laser should be carefully adjusted to produce an asymmetric hot-spots distribution.

As it was mentioned above, the Fano resonance of the APH is polarization-dependent. Changing the polarization can modulate the Fano resonance of the APH, and thus, control the distribution of the near-field hot-spots. It is necessary to consider the optimized sensing contrast under different excitation polarizations. In Fig. 4, we present the result of the maximum normalized TPL sensing signals under typical input polarizations when the protein moves at different directions θ towards the center of the APH. As can be seen from this figure, the maximum normalized TPL contrast can be maintained higher than four orders of magnitude in broad ranges of the

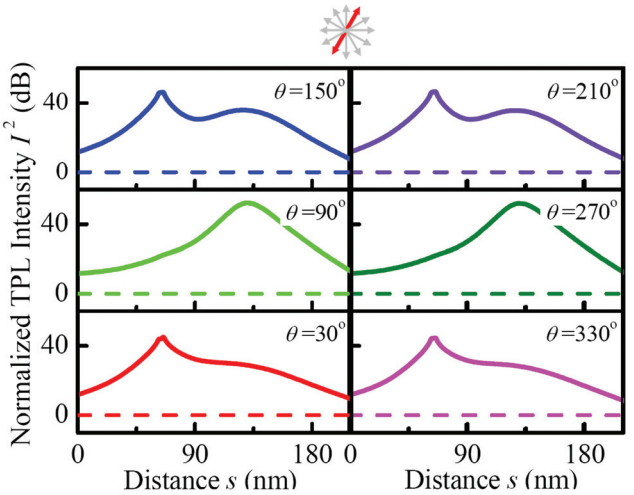

Fig. 3 Evolutions of the normalized TPL intensity of the protein from different directions approaching the center of the APH. The corresponding evolutions of the TPL intensity from the APH are shown by dash lines. The normalized TPL is evaluated by using the eqn (2) in the Method section. The input polarization (P = 30°) is indicated by the red double arrows of the inset.

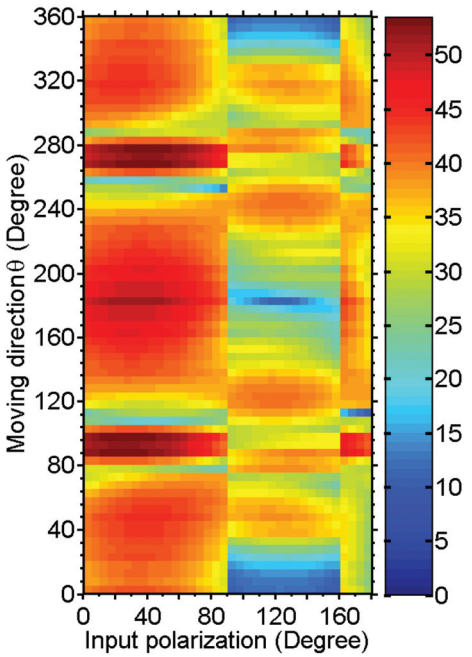

Fig. 4 The maximum TPL sensing signals under different excitation polarizations when the protein moves at different directions θ towards the center of the APH. The color scale is in logarithmic scale.

excitation polarizations and moving directions, demonstrating the working tolerance of our scheme. It should be pointed out that the normalized TPL signals of the protein are symmetric referring to θ = 180°, when the input polarization is equal to 30° and 120°. These two cases cannot be used to trace the protein. It should be pointed out that the electric field distributions shown in Fig. 1(d) and (e) are exponentially decay along APH's surface normal. Therefore, it can be used to realize three-dimensional sensing near the APH rather than the representative two-dimensional case shown in Fig. 2.

We also consider a more realistic case with fabrication impurities. We model the inaccuracies in the fabrication process with ±4 nm diameter variation according to the state-of-the-art fabrication technology. The calculated results in Fig. 5 demonstrates that the proposed TPL sensing strategy is still robust when moderate fabrication imperfect is taken into account. The variation of TPL signal is closed to the ideal structure. It should be pointed out that non-circular gold disks with ±4 nm shape deformation might also affect the position sensing sensitivity similar to the diameter variation. Surface roughness of the gold film might also degrade the sensing performance. Attention should be paid into the whole fabrication process, which can promise a robust Fano resonance with an asymmetry mode profile.[43] Quenching effect would reduce the TPL from the protein and affect the contrast of the sensing signal. This effect is minimized when the distance between the plasmonic structure and the protein is larger than 5 nm.[69] In order to show that our sensing scheme is reliable, we present the results of the normalized TPL evolutions when the protein is moving in a plane, which is 6 nm above the metallic surface, in the ESI Fig. S3.† As can be seen from these results, the evolutions of the normalized TPL signal are similar to those ones presented in Fig. 2(b) while the maximum contrast of the TPL signal can approach four orders of magnitude. Furthermore, the Fano resonant enhanced absorption (*i.e.* excitation enhancement) is out of the spectrum of the interband transition of gold, which would release the quenching effect

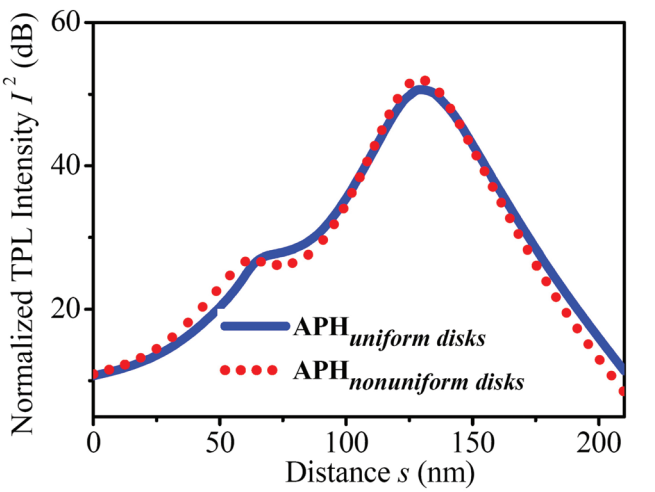

Fig. 5 Evolutions of normalized TPL intensity of the protein when it moves towards the center of the APH composed of a uniform sized naondisks (black dot line) and the APH composed of nonuniform sized nanodisks (red short dot line), respectively. The moving diretion θ of the protein is chosen to be 90° and the deviation of the nonuniform sized nanodisks is set to be ±4 nm.

caused by LSPR damping.[70] All these results further strength the proposed Fano resonance enhanced TPL sensing strategy. Further increasing the constituents of the oligomer will produce asymmetry modes with more complex near field hot-spot distribution, which might be useful in enhancing the spatial resolution of the sensing for a given degree of TPL detection accuracy. All presented results demonstrate a robust single protein sensing strategy using Fano resonance enhanced TPL.

3 Conclusions

In conclusion, we demonstrate the single protein sensing by using the Fano resonance enhanced TPL with a gold APH. We show that the polarization-dependent plasmonic Fano resonance system provides asymmetric near-field hot-spot distributions, which can facilitate the tracing of a single protein. The near-field interaction between the protein and the plasmonic Fano resonant modes would result in a giant electric field enhancement in the protein. Therefore, the protein's TPL excitation rate is greatly enhanced. By monitoring the TPL intensities from the protein when it moves along different directions, distinct fluctuation properties of the TPL signal can be used to obtain the high sensitivity single protein detection, whose sensitivity for a protein's position change can be five orders of magnitude better than the conventional linear approach. We also show that the proposed sensing strategy is robust to the realistic fabrication errors. Therefore, we believe that our results may stimulate certain experimental advances in the related field. Furthermore, the proposed strategy can be generalized to similar applications in biochemistry and biomolecular diagnostics. In particular, we hope that it can facilitate the study of biokinetics in the single molecule level and shed new light on the well-studied plasmonic oligomer structures.

4 Methods

We employ the three-dimensional finite-difference time-domain (FDTD) method to model the single protein sensing.[71] The FDTD method has widely been used to model the plasmonic nanostructure enhanced florescence which is also validated by experiments.[72–74] It is shown that the TPL is proportional to the fourth power of electric field in the fluorescent object and the total TPL power will be correlated to the integral of $|E|^4$ over the volume of the object.[75–77] We use a plane wave with its k-vector normal to the APH mimicking the excitation condition of a focus laser at its focal plane [see Fig. 1(a)], since the focus spot (1 μm in diameter when a 100 objective lens is applied) is about 3 times larger than the size of the APH. The complex and dispersive permittivity of gold used in FDTD is taken from the experimental data of Johnson and Christy.[78] We use the TPL of the same structure immersed in water (n = 1.33) for the TPL normalization. We also consider the substrate effect (n = 1.55) in the numerical calculation.[79,80] We use a sphere with 10 nm diameter to model the GFP, although it might be smaller than this one in realistic case. Because we use the normalized TPL to account for the position change of the protein, the small discrepancy of the protein size between the modelling one and the real GFP would not bring quantitative differences. It should be noted that the proposed sensing strategy is feasible for different morphologies of the subwavelength protein. The simulations are performed based on a discrete grid with a size of 1 nm to take a balance between accuracy and efficiency. Perfect match layers are used to truncate the modelling domain and avoid reflection from all boundaries.

We use four electric dipoles with random orientations placed randomly in the gaps among gold nanodisks to locally excite the subradiant states. The bandwidth of the Gaussian pulses is about 80 nm which is centered at the Fano resonance frequency. By doing Fourier transform of the recorded time evolution at the target spatial grids in a suitable time window where the exponential decay rate is different from the Gaussian one, we can identify the targeted subradiant mode by comparing the resulted frequency with the one in Fig. 1(b). Then, we can obtain the quasi-steady states which can qualitatively represent the considered subradiant modes of the APH. It should be noted that we only present the directions of the constituent dipoles because we apply different length of the time windows to different subradiant modes owing to their distinct life time.

The normalized TPL (NTPL) of the protein shown in Fig. 1(a) can be evaluated by:

$$I_{\text{protein}}^{\text{NTPL}} = \frac{I_{\text{detection}}^{\text{TPL}}}{I_{\text{in water}}^{\text{TPL}}} = \frac{\int_{\text{protein}} |E(\lambda_{\text{ex}}, r)/E_{\text{i}}|^4 \mathrm{d}V \int_{\text{protein}} |E(\lambda_{\text{em}}, r)/E_{\text{i}}|^2 \mathrm{d}V}{\int_{\text{protein}} |E(\lambda_{\text{ex}}, r)_{\text{bare}}/E_{\text{i}}|^4 \mathrm{d}V \int_{\text{protein}} |E(\lambda_{\text{em}}, r)_{\text{bare}}/E_{\text{i}}|^2 \mathrm{d}V} \quad (1)$$

where $E(\lambda_{\text{ex}}, r)$ and $E(\lambda_{\text{em}}, r)$ are the amplitudes of the electric fields at the excitation wavelength and the emission wavelength, respectively.

E_{i} is the amplitude of the incident electric field. $I_{\text{detection}}^{\text{TPL}}$ is the target TPL signal of the system being detected while $I_{\text{in water}}^{\text{TPL}}$ stands for the TPL used for the normalization. $\mathrm{d}V$ is the volume element. In a case that the emission wavelength, (for example, λ_{em} = 510 nm) is far away from the Fano resonant frequency of the APH, there is negligible variation of the volume integration of electric intensity $\int_{\text{Au}} |E(\lambda_{\text{em}}, r)|^2 \mathrm{d}V$ when a protein moves towards the center of the gold APH. To be more concrete, Fig. S4(a) in the ESI† shows the normalized volume integration of the square of the electric intensity $\left(\int_{\text{protein}} |E(\lambda_{\text{ex}}, r)|^4 \mathrm{d}V\right)$ and volume integration of electric intensity $\left(\int_{\text{protein}} |E(\lambda_{\text{em}}, r)|^2 \mathrm{d}V\right)$ of the protein when it moves towards the center of the APH along the direction θ = 90° at the excitation (920 nm) and emission (510 nm) wavelengths, respectively. Since the emission frequency is far from the Fano

resonant frequency of the APH, the variation of the integral $\int_{\text{protein}} |E(\lambda_{\text{em}}, r)|^2 \mathrm{d}V$ at emission wavelength is very small compared with the excitation one. The results at the emission wavelengths of yellow and red fluorescent proteins are similar and not shown here. Therefore, the normalized TPL of the protein volume can be further simplified as:

$$I_{\text{protein}}^{\text{NTPL}} = \frac{\int_{\text{protein}} |E(\lambda_{\text{ex}}, r)/E_{\text{i}}|^4 \mathrm{d}V}{\int_{\text{protein}} |E(\lambda_{\text{ex}}, r)_{\text{bare}}/E_{\text{i}}|^4 \mathrm{d}V} \quad (2)$$

where $E(\lambda_{\text{ex}}, r)_{\text{bare}}$ stands for the electric field inside the protein when the protein is immersed in water. We can obtain the normalized TPL of the gold APH in a similar way as eqn (2). The normalized TPL evolutions obtained by directly evaluate eqn (1) is plotted in the ESI Fig. S4(b)† for comparison. As can be seen from this figure, the approximation is reasonable.

Because the three-dimensional FDTD simulation is very time consuming if one uses the above mentioned method for optimising the sensing sensitivity. In the following, we use an efficient while robust method to calculate the maximum TPL sensing signals under different excitation polarizations when the protein moves at different directions θ towards the center of the APH. For a single protein with small radius $R \ll \lambda$ immersed in water and interacting with the APH, we can assume that the electric field inside its volume is homogeneous and is equal to:

$$E_{\text{protein}} = \frac{3\varepsilon_{\text{water}}}{2\varepsilon_{\text{water}} + \varepsilon_{\text{protein}}} E_{\text{local}} \quad (3)$$

We can obtain the relationship between the electric field inside the protein and the local field of the APH as:

$$E_{\text{protein}} = \alpha E_{\text{local}} \quad (4)$$

where α = 0.92 in our case. Therefore, the enhancement of the TPL of the protein can be greatly simplified as

$$\eta_{\text{TPL}} = \frac{\int_{\text{protein}} |E(\lambda_{\text{ex}}, r)/E_{\text{i}}|^4 \mathrm{d}V}{\int_{\text{protein}} |E(\lambda_{\text{ex}}, r)_{\text{bare}}/E_{\text{i}}|^4 \mathrm{d}V} = \frac{|E_{\text{with APH}}|^4}{|E_{\text{without APH}}|^4} \quad (5)$$

where $E_{\text{with APH}}$ and $E_{\text{without APH}}$ are the electric fields at the spatial grids above the APH in the calculation domain with and without the APH, respectively.

Acknowledgements

The authors thank the financial support from National Natural Science Foundation of China (Grant No. 11304047), Natural Science Foundation of Guangdong Province (Grant No. 2014A030313376 and S2012040007719). Y. Xu appreciates the financial support from the Fundamental Research Funds for the Central Universities (Grant No. 21615449) and FDYT in Higher Education of Guangdong Province (Grant No. 2013LYM0067). The work of A. E. Miroshnichenko was supported by the Australian Research Council through the Future Fellowship program (FT110100037). H. Deng acknowledges the support from the Science and Technology Program of Guangzhou (Grant No. 201505041143348).

References

1 S. H. Leuba and J. Zlatanova, *Biology at the Single Molecule Level*, Pergamon Press, New York, 2001.
2 W. E. Moerner and M. Orrit, *Science*, 1999, **283**, 1670–1676.
3 C. B. Rosen and D. Rodriguez-Larrea, *Nat. Biotechnol.*, 2014, **32**, 179–181.
4 S. Kang, A. F. Nieuwenhuis, K. Mathwig, D. Mampallil and S. G. Lemay, *ACS Nano*, 2013, **7**, 10931–10937.
5 V. G. Kravets, F. Schedin, R. Jalil, L. Britnell, R. V. Gorbachev, D. Ansell, B. Thackray, K. S. Novoselov, A. K. Geim, A. V. Kabashin and A. N. Grigorenko, *Nat. Mater.*, 2013, **12**, 304–309.
6 M. Orrit and J. Bernard, *Phys. Rev. Lett.*, 1990, **65**, 2716–2719.
7 S. Nie and S. R. Emory, *Science*, 1997, **275**, 1102–1106.
8 A. Gaiduk, M. Yorulmaz, P. V. Ruijgrok and M. Orrit, *Science*, 2010, **330**, 353–356.
9 P. Kukura, M. Celebrano, A. Renn and V. Sandoghdar, *J. Phys. Chem. Lett.*, 2010, **1**, 3323–3327.
10 L. Wei, S. Lu, S. Chong, R. Roy, G. R. Holtom and X. S. Xie, *Nature*, 2009, **461**, 1105–1109.
11 A. M. Armani, R. P. Kulkarni, S. E. Fraser, R. C. Flagan and K. J. Vahala, *Science*, 2007, **317**, 783–787.
12 V. R. Dantham, S. Holler, C. Barbre, D. Keng, V. Kolchenko and S. Arnold, *Nano Lett.*, 2013, **13**, 3347–3351.
13 H. Yang, M. Cornaglia and M. A. M. Gijs, *Nano Lett.*, 2014, **15**, 1730–1735.
14 S. Lal, S. Link and N. J. Halas, *Nat. Photonics*, 2007, **1**, 641–648.
15 J. N. Anker, W. P. Hall, O. Lyandres, N. C. Shah, J. Zhao and R. P. Van Duyne, *Nat. Mater.*, 2008, **7**, 442–453.
16 M. E. Stewart, C. R. Anderton, L. B. Thompson, J. Maria, S. K. Gray, J. A. Ogers and R. G. Nuzzo, *Chem. Rev.*, 2008, **108**, 494–521.
17 K. M. Mayer and J. H. Hafner, *Chem. Rev.*, 2011, **111**, 3828–3857.
18 S. Zhang, L. Chen, Y. Huang and H. Xu, *Nanoscale*, 2013, **5**, 6985–6991.
19 J. Xian, L. Chen, H. Niu, J. Qu and J. Song, *Nanoscale*, 2014, **6**, 13994–14001.
20 F. Tam, G. P. Goodrich, B. R. Johnson and N. J. Halas, *Nano Lett.*, 2007, **7**, 496–501.
21 R. Bardhan, N. K. Grady, J. R. Cole, A. Joshi and N. J. Halas, *ACS Nano*, 2009, **3**, 744–752.
22 S. Khatua, P. M. R. Paulo, H. Yuan, A. Gupta, P. Zijlstra and M. Orrit, *ACS Nano*, 2014, **8**, 4440–4449.
23 G. Lu, L. Hou, T. Zhang, J. Liu, H. Shen, C. Luo and Q. Gong, *J. Phys. Chem. C*, 2012, **116**, 25509–25516.

24 G. Lu, T. Zhang, W. Li, L. Hou, J. Liu and Q. Gong, *J. Phys. Chem. C*, 2011, **115**, 15822–15828.
25 G. Lu, L. Hou, T. Zhang, W. Li, J. Liu, P. Perriat and Q. Gong, *J. Phys. Chem. C*, 2011, **115**, 22877–22885.
26 N. S. Abadeer, M. R. Brennan, W. L. Wilson and C. J. Murphy, *ACS Nano*, 2014, **8**, 8392–8406.
27 J. O. Arroyo, J. Andrecka, K. M. Spillane, N. Billington, Y. Takagi, J. R. Sellers and P. Kukura, *Nano Lett.*, 2014, **14**, 2065–2070.
28 L. Chen, G. C. Li, G. Y. Liu, Q. F. Dai, S. Lan, S. L. Tie and H. D. Deng, *J. Phys. Chem. C*, 2013, **117**, 20146–20153.
29 A. E. Miroshnichenko, S. Flach and Y. S. Kivshar, *Rev. Mod. Phys.*, 2010, **82**, 2257–2298.
30 B. Luk'yanchuk, N. I. Zheludev, S. A. Maier, N. J. Halas, P. Nordlander, H. Giessen and C. T. Chong, *Nat. Mater.*, 2010, **9**, 707–715.
31 M. Rahmani, B. Luk'yanchuk and M. Hong, *Laser Photonics Rev.*, 2012, **7**, 329–349.
32 Z. Fang and X. Zhu, *Adv. Mater.*, 2013, **25**, 3840–3856.
33 Z. J. Yang, Z. H. Hao, H. Q. Li and Q. Q. Wang, *Nanoscale*, 2014, **6**, 4985–4997.
34 Y. Shen, J. H. Zhou, T. R. Liu, Y. T. Tao, R. B. Jiang, M. X. Liu, G. H. Xiao, J. H. Zhu, Z. K. Zhou, X. H. Wang, C. J. Jin and J. F. Wang, *Nat. Commun.*, 2013, **4**, 2381.
35 C. Ayala-Orozco, J. G. Liu, M. W. Knight, Y. Wang, J. K. Day, P. Nordlander and N. J. Halas, *Nano Lett.*, 2014, **14**, 2926–2933.
36 Z. K. Zhou, X. N. Peng, Z. J. Yang, Z. S. Zhang, M. Li, X. R. Su, Q. Zhang, X. Shan, Q. Q. Wang and Z. Zhang, *Nano Lett.*, 2011, **11**, 49–55.
37 H. D. Deng, J. L. Xu and Y. Xu, *Phys. Status Solidi RRL*, 2014, **8**, 427–430.
38 F. Le, D. W. Brandl, Y. A. Urzhumov, H. Wang, J. Kundu, N. J. Halas, J. Aizpurua and P. Nordlander, *ACS Nano*, 2008, **2**, 707–718.
39 F. Hao, Y. Sonnefraud, P. V. Dorpe, S. A. Maier, N. J. Halas and P. Nordlander, *Nano Lett.*, 2008, **8**, 3983–3988.
40 J. A. Fan, K. Bao, J. Bao, R. Bardhan, N. J. Halas, V. N. Manoharan, P. Nordlander and F. Capasso, *Science*, 2010, **328**, 1135–1138.
41 J. A. Fan, K. Bao, C. Wu, J. Bao, R. Bardhan, N. J. Halas, V. N. Manoharan, G. Shvets, P. Nordlander and F. Capasso, *Nano Lett.*, 2010, **10**, 4680–4685.
42 M. Hentschel, M. Saliba, R. Vogelgesang, H. Giessen, A. P. Alivisatos and N. Liu, *Nano Lett.*, 2010, **10**, 2721–2726.
43 J. B. Lassiter, H. Sobhani, J. A. Fan, J. Kundu, F. Capasso, P. Nordlander and N. J. Halas, *Nano Lett.*, 2010, **10**, 3184–3189.
44 S. N. Sheikholeslami, A. Garcia-Etxarri and J. A. Dionne, *Nano Lett.*, 2011, **11**, 3927–3934.
45 M. Hentschel, D. Dregely, R. Vogelgesang, H. Giessen and N. Liu, *ACS Nano*, 2011, **5**, 2042–2050.
46 D. Dregely, M. Hentschel and H. Giessen, *ACS Nano*, 2011, **5**, 8202–8211.
47 J. B. Lassiter, H. Sobhani, M. W. Knight, W. S. Mielczarek, P. Nordlander and N. J. Halas, *Nano Lett.*, 2012, **12**, 1058–1062.
48 A. E. Miroshnichenko and Y. S. Kivshar, *Nano Lett.*, 2012, **12**, 6459–6463.
49 Y. Cui, J. Zhou, V. A. Tamma and W. Park, *ACS Nano*, 2012, **6**, 2385–2393.
50 S. D. Liu, Z. Yang, R. P. Liu and X. Y. Li, *ACS Nano*, 2012, **6**, 6260–6271.
51 J. Sancho-Parramon and S. Bosch, *ACS Nano*, 2012, **6**, 8415–8423.
52 M. Rahmani, D. Y. Lei, V. Giannini, B. Lukiyanchuk, M. Ranjbar, T. Y. F. Liew, M. Hong and S. A. Maier, *Nano Lett.*, 2012, **12**, 2101–2106.
53 F. Wen, J. Ye, N. Liu, P. Van Dorpe, P. Nordlander and N. J. Halas, *Nano Lett.*, 2012, **12**, 5020–5026.
54 Z. Y. Fang, Y. Wang, Z. Liu, A. Schlather, P. M. Ajayan, F. H. L. Koppens, P. Nordlander and N. J. Halas, *ACS Nano*, 2012, **6**, 10222–10228.
55 Z. Y. Fang, Z. Liu, Y. Wang, P. M. Ajayan, P. Nordlander and N. J. Halas, *Nano Lett.*, 2012, **12**, 3808–3813.
56 M. Rahmani, E. Yoxall, B. Hopkins, Y. Sonnefraud, Y. Kivshar, M. Hong, C. Phillips, S. A. Maier and A. E. Miroshnichenko, *ACS Nano*, 2013, **7**, 11138–11146.
57 Y. Zhang, F. Wen, Y. R. Zhen, P. Nordlander and N. J. Halas, *Proc. Natl. Acad. Sci. U. S. A.*, 2013, **110**, 9215–9219.
58 K. Thyagarajan, J. Butet and O. J. F. Martin, *Nano Lett.*, 2013, **13**, 1847–1851.
59 V. A. Tamma, Y. H. Cui, J. H. Zhou and W. N. Park, *Nanoscale*, 2013, **5**, 1592–1602.
60 Y. Wang, Z. Li, K. Zhao, A. Sobhani, X. Zhu, Z. Fang and N. J. Halas, *Nanoscale*, 2013, **5**, 9897–9901.
61 A. Nazir, S. Panaro, R. P. Zaccaria, C. Liberale, F. D. Angelis and A. Toma, *Nano Lett.*, 2014, **14**, 3166–3171.
62 B. Hopkins, W. Liu, A. E. Miroshnichenko and Y. S. Kivshar, *Nanoscale*, 2013, **5**, 6395–6403.
63 G. Grinblat, M. Rahmani, E. Cortés, M. Caldarola, D. Comedi, S. A. Maier and A. V. Bragas, *Nano Lett.*, 2014, **14**, 6660–6665.
64 J. Butet and O. J. F. Martin, *Nanoscale*, 2014, **6**, 15262–15270.
65 M. D. Wissert, K. S. Ilin, M. Siegel, U. Lemmer and H. J. Eisler, *Nano Lett.*, 2010, **10**, 4161.
66 W. L. Chen, F. C. Lin, Y. Yang Lee, F. C. Li, Y. M. Chang and J. S. Huang, *ACS Nano*, 2014, **8**, 9053.
67 H. D. Deng, G. C. Li, Q. F. Dai, M. Ouyang, S. Lan, V. A. Trofimov and T. M. Lysak, *Nanotechnology*, 2013, **24**, 075201.
68 J. E. Donehue, E. Wertz, C. N. Talicska and J. S. Biteen, *J. Phys. Chem. C*, 2014, **118**, 15027–15035.
69 H. Szmacinski, R. Badugu and J. R. Lakowicz, *J. Phys. Chem. C*, 2010, **114**, 21142–21149.
70 K. Sugawa, T. Tamura, H. Tahara, D. Yamaguchi, T. Akiyama, J. Otsuki, Y. Kusaka, N. Fukuda and H. Ushijima, *ACS Nano*, 2013, **7**, 9997–10010.

71 A. Taflove and S. C. Hagness, *Computational Electrodynamics: The Finite-Difference Time-Domain Method*, Artech House, Boston, 3rd edn, 2005.
72 J. Zhang, Y. Fu, M. H. Chowdhury and J. R. Lakowicz, *Nano Lett.*, 2007, **7**, 2101–2107.
73 G. W. Lu, W. Li, T. Zhang, S. Yue, J. Liu, L. Hou, Z. Li and Q. Gong, *ACS Nano*, 2012, **6**, 1438–1448.
74 G. W. Lu, J. Liu, T. Zhang, H. Shen, P. Perriat, M. Martini, O. Tillement, Y. Gu, Y. He, Y. Wang and Q. Gong, *Nanoscale*, 2013, **5**, 6545–6551.
75 P. J. Schuck, D. P. Fromm, A. Sundaramurthy, G. S. Kino and W. E. Moerner, *Phys. Rev. Lett.*, 2005, **94**, 017402.
76 P. Ghenuche, S. Cherukulappurath, T. H. Taminiau, N. F. Hulst and R. Quidant, *Phys. Rev. Lett.*, 2008, **101**, 116805.
77 A. McLeod, A. Weber-Bargioni, Z. Zhang, S. Dhuey, B. Harteneck, J. B. Neaton, S. Cabrini and P. James Schuck, *Phys. Rev. Lett.*, 2011, **106**, 037402.
78 P. B. Johnson and R. W. Christy, *Phys. Rev. B: Solid State*, 1972, **6**, 4370–4379.
79 S. Zhang, K. Bao, N. J. Halas, H. Xu and P. Nordlander, *Nano Lett.*, 2011, **11**, 1657–1663.
80 H. Chen, L. Shao, T. Ming, K. C. Woo, Y. C. Man, J. Wang and H. Q. Lin, *ACS Nano*, 2011, **8**, 6754–6763.